Improved Flux-Weakening Control of IPMSMs Based on Torque Feedforward Technique

Yuzheng Chen, Xiaoyan Huang, *Member, IEEE*, Jun Wang, *Student Member, IEEE*, Feng Niu, *Member, IEEE*, Jian Zhang, Youtong Fang, *Senior Member, IEEE*, and Lijian Wu, *Senior Member, IEEE*

***Abstract*—A flux-weakening control algorithm with an improved stator flux linkage command's adjustment part of interior permanent magnet synchronous motors is proposed in this paper. The current commands are derived from lookup tables, which consider variation of motor parameters. The merits of this algorithm are the maximization of torque and high torque stability. Experimental results are demonstrated to verify the effectiveness of the proposed algorithm.**

***Index Terms*—Flux-weakening, interior permanent magnet synchronous motors (IPMSMs), lookup table (LUT), torque feedforward.**

NOMENCLATURE

$*$	Superscript of command values.
u_d, u_q	*d–q* components of stator voltages.
i_d, i_q	*d–q* components of stator currents.
L_d, L_q	*d–q* components of stator selfinductance.
R_s	Stator resistance.
ω_e	Electrical rotor speed.
λ_f	Permanent-magnet flux linkage.
λ_d	*d*-axis stator flux linkage.
λ_q	*q*-axis stator flux linkage.
λ_s	Stator flux linkage.
T_e	Electromagnetic torque.
P	Pole numbers.
$I_{s\_\max}$	Magnitude of maximum phase current.
V_s	Magnitude of stator phase voltage.
$V_{\rm dc}$	DC-link voltage of inverter.

I. INTRODUCTION

INTERIOR permanent magnet synchronous motors (IPMSMs) have many merits such as high efficiency and power density [1], [2]. When operating speed goes beyond

Manuscript received July 28, 2017; revised October 19, 2017 and January 2, 2018; accepted February 20, 2018. Date of publication February 28, 2018; date of current version September 28, 2018. This work was supported by the National Natural Science Foundation of China under Grant 51477149 and Grant U143420005. Recommended for publication by Associate Editor I. Slama-Belkhodja. *(Corresponding author: Xiaoyan Huang.)*

The authors are with the College of Electrical Engineering, Zhejiang University, Hangzhou 310027, China (e-mail:

voltage limit equation, and torque equation are quadratic and the analytical solutions of their intersections are difficult to obtain. A feasible solution is only using voltage limit equation to calculate *q*-axis current commands. As a tradeoff, *d*-axis current command is derived from a PI regulator [17]. On the contrary, another feasible solution obtains *q*-axis current command from a PI regulator and uses analytical equation of maximum torque per voltage (MPTV) to calculate *d*-axis current command [18], [19]. With the rapid development of microprocessors, complex online mathematical computation is achievable. In [20] and [21], iterative method is used to calculate the numerical solution of quartic equation online, which is the optimal current operating point in the flux-weakening region. To overcome parameter nonlinearity, *d*-axis and *q*-axis inductances are obtained from LUTs.

In addition to the online calculation, another alternative method is using LUTs to store all the current commands in the flux-weakening region. Several papers have researched on how to construct current LUTs [22]–[24]. In [22], the finite element results are used to construct LUT. Its drawback is that the structure of stator and rotor must be obtained. On the contrary, the method proposed in [23] uses measured voltages, currents, and speed to construct LUTs. In addition, maximum torque per ampere (MTPA) and MTPV lines based on measured data are used as LUTs' boundaries. The choosing criteria of optimal current operating point is proposed as well. In [24], a replacement method of invalid table elements is introduced in detail.

There are two kinds of LUTs in previous papers. One uses torque command T_e^* and rotor speed ω_e as LUT's searching indexes [23], [25]–[27], the other uses torque command T_e^* and stator flux linkage command λ_s^* [28]–[32]. In [27], minimum currents under different speed and torque conditions are obtained through convex optimization to construct $T_e^* - \omega_e$ LUT. However, in [23], the maximum speed and torque at every operating point are calculated through motor equations. The two methods have the same drawback that the maximum voltage vector is fixed. However, the dc voltage will change with dc current if it is provided by a diode rectifier. Therefore, the assumption of unchanged maximum voltage vector is not feasible.

As another kind of LUT, $T_e^* - \lambda_s^*$ LUT attracts more research attention. Although λ_s^* cannot be measured directly like ω_e, it can reflect the saturation of voltage more accurately. In [29] and [30], λ_s^* consists of two parts. One is proportional to $V_{\rm dc}/\omega_e$ as main λ_s^*, the other, as compensation of λ_s^*, comes from a PI regulator whose input is the error between modulation index (MI) and MI reference. The estimated torque is used as feedback to achieve more precise torque control. However, the MI reference is set to an unchanged value, which limits the maximum utilization of dc-link voltage. In [28] and [31], the difference between reference voltages before and after overmodulation is used and low-pass filters are added to avoid saturation of current regulator. However, this proposed algorithm does not have the feedback of dc-link voltage, which cannot cope with the fluctuation of dc voltage. In [32], only i_q^* is obtained from LUT, and i_d^* is adjusted using a PI regulator whose input is the difference between composite voltage command and its maximum reference. In fact, all methods based on $T_e^* - \lambda_s^*$ LUT are actually a mix of feedback and feedforward. They have the merit of robustness owed by feedback control as well as the merit of fast transient performance owed by feedforward control. Because of the superiority of $T_e^* - \lambda_s^*$ LUT, it is used for the proposed flux-weakening algorithm in this paper.

In this paper, an improved flux-weakening control algorithm of IPMSMs based on torque feedforward technique is proposed to generate large and stable torque in the flux-weakening region. The $T_e^* - \lambda_s^*$ LUT is adopted because of its superiority and the adaptive adjustment algorithm of λ_s^* is the innovation point of this paper, which can maximizes the output torque as well as the utilization of dc voltage. This paper is organized as follows. In Section II, the mathematical model of IPMSM and the structure of torque feedforward control system is introduced. In Section III, the principle and structure of stator flux linkage adjustment is proposed. In Section IV, the LUTs construction, current regulators, and voltage overmodulation are introduced. Finally, simulation and experimental results are shown in Sections V and VI, respectively.

II. IPMSM Model and Control System Structure

A. IPMSM Model and Operating Boundaries

In a rotor reference frame, the mathematical model of IPMSM can be described as the following equations [29], [30], [33], and [34].

Steady-state voltage equations

$$u_d = R_s i_d - \omega_e \lambda_q \tag{1}$$

$$u_q = R_s i_q + \omega_e \lambda_d. \tag{2}$$

Steady-state stator flux linkage equations

$$\lambda_d = L_d i_d + \lambda_f \tag{3}$$

$$\lambda_q = L_q i_q \tag{4}$$

$$\lambda_s = \sqrt{\lambda_d^2 + \lambda_q^2}. \tag{5}$$

Torque equation

$$T_e = \frac{3}{2}\frac{P}{2}\left[\lambda_f i_q + (L_d - L_q)\, i_d i_q\right]. \tag{6}$$

MTPA

$$i_d = \frac{\lambda_f}{2\,(L_d - L_q)} - \sqrt{\frac{{\lambda_f}^2}{4{(L_d - L_q)}^2} + {i_q}^2}. \tag{7}$$

Current limitation equation

$${i_d}^2 + {i_q}^2 = I_{s\_\max}^2. \tag{8}$$

Stator flux linkage equation

$$\lambda_s = \frac{V_s}{\omega_e} = \sqrt{(L_q i_q)^2 + (L_d i_d + \lambda_f)^2}. \tag{9}$$

In a constant torque region, current operating points are located on MTPA curve for minimizing the copper loss. In the flux-weakening region, because of the limitation of dc-link voltage, the magnitude of i_d has to increase. The larger increase of i_d will lead to higher copper loss. However, if i_d does not increase large enough, the output of current regulator will saturate, aggravating torque fluctuation. Therefore, there is a tradeoff between the

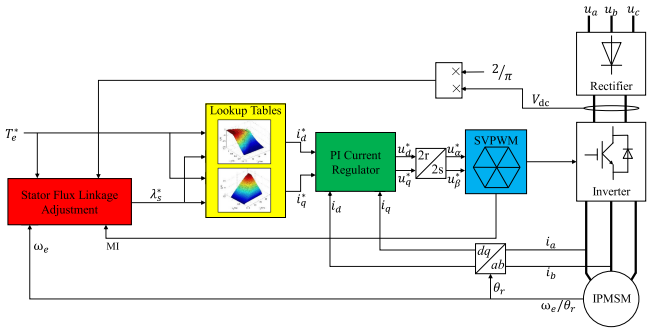

Fig. 1. Torque feedforward control system.

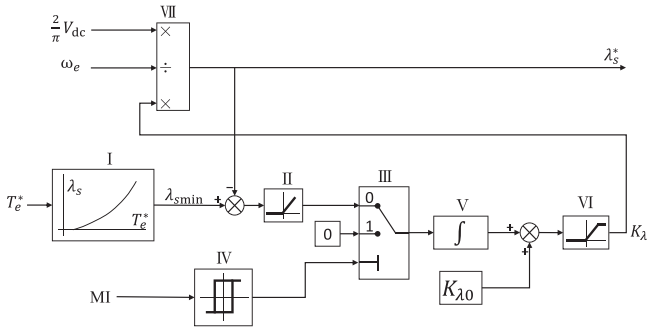

Fig. 2. Proposed stator flux linkage commands adjustment algorithm.

motor efficiency and the torque stability in the flux-weakening region.

B. Torque Feedforward Control System Structure

The whole flux-weakening control system is shown in Fig. 1, which contains four main control blocks: stator flux linkage adjustment, LUTs, PI current regulator, and space vector pulse-width modulation (SVPWM). The stator flux linkage adjustment block introduces a dynamic adjustable flux linkage coefficient K_λ, which adjusts stator flux linkage according to several variables like MI, torque commands, rotor speed, and dc-link voltage. LUTs block searches $T_e^* - \lambda_s^*$ LUT for current commands. PI current regulator uses typical PI regulator with back electromotive force (EMF) decouple and antiwindup. SVPWM block contains overmodulation algorithm, achieving a smooth transition from SVPWM to a six-step mode.

III. Stator Flux Linkage Commands Adjustment Algorithm

The proposed stator flux linkage commands adjustment algorithm, illustrated in Fig. 2, plays a very important role because it generates the stator flux linkage commands, which is one of the inputs of LUT. Compared with the conventional algorithm [28], [29], whose flux linkage commands are the sum of two parts (main flux linkage and compensate flux linkage), the proposed algorithm multiplies the maximum flux linkage by a changeable coefficient (K_λ), which will be changed automatically to generate potentially maximum torque without losing control of the current regulator. The maximum flux linkage is shown in

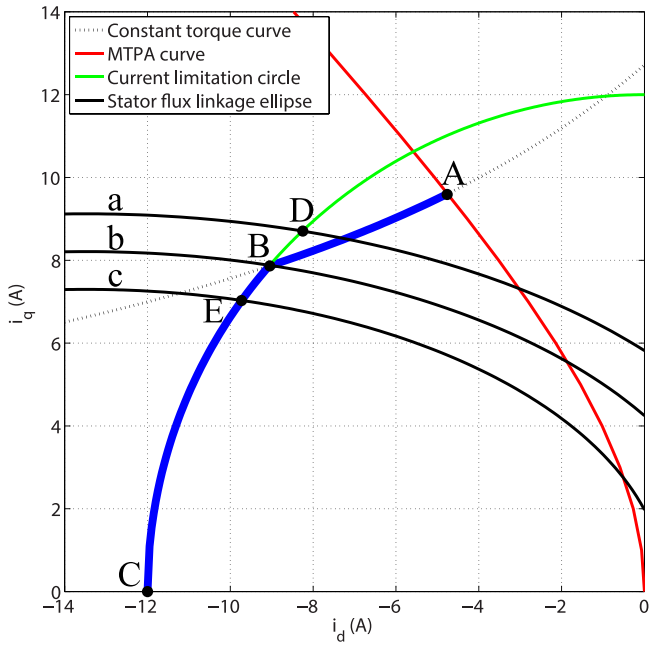

Fig. 3. Operating points of d-, q-axis currents in the flux-weakening region.

(10), and the numerator of it represents the fundamental wave magnitude of six-step voltage, which is the maximum of inverter output

$$\lambda_{s\max} = \frac{\frac{2}{\pi}V_{\rm dc}}{\omega_e}. \tag{10}$$

For an IPMSM with finite constant power speed ratio [8], [9], the flux-weakening region is divided into two parts: constant torque part like "AB" and current limitation circle part like "BC" are shown in Fig. 3. If the coefficient (K_λ) in Fig. 2 is set to the maximum value 1, the corresponding stator flux linkage ellipse is like line "a." Although the intersection "D" can produce larger torque than that point "B" can produce, point "D" is unreachable because of the resistance voltage drop and inverter-distorted voltage. If the current regulator utilizes the current commands on point "D," it will cause the saturation of current regulator and lead to the unstability of the output torque. Traditionally, in order to obtain the stable output torque, a sacrificed flux linkage like line "c" is practically used, which leads to the maximum torque operating point located at point "E."

In this paper, a changeable K_λ is utilized to adjust stator flux linkage command, aiming at producing the largest and stable output torque. According to the proposed algorithm in Fig. 2, an initial coefficient $K_{\lambda 0}$ will increase to an optimal value through an integral regulator, which means the corresponding stator flux linkage ellipse will expand from line "c" to line "b," and the point of maximum torque changes from point "E" to point "B." So, compared with the points "D" and "E," point "B" is the optimal selection.

The block I in Fig. 2 is a polynomial-fit function between λ_s and T_e, which can calculate the minimum λ_s for a specific torque command. Because the intersection point of constant torque curve and current limitation circle has the minimum stator

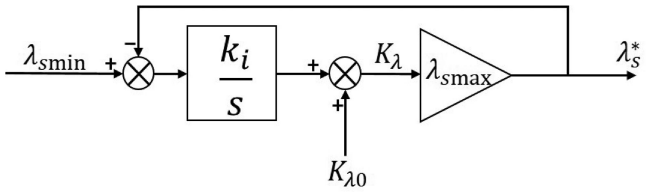

Fig. 4. Simplified proposed stator flux linkage commands adjustment algorithm.

flux linkage for each torque command, λ_s is calculated using stator flux linkage (9) and T_e is measured by torque sensor at every current operating point on current limitation circle. The operation procedure of proposed stator flux linkage commands adjustment algorithm in Fig. 2 is depicted as follows.

1) Find the minimum stator flux linkage $\lambda_{s\min}$ through block I. The $\lambda_{s\min}$ represents the minimum stator flux linkage this motor can achieve under the specific torque command.
2) Compare $\lambda_{s\min}$ with stator flux linkage command λ_s^*. If $\lambda_s^* > \lambda_{s\min}$, block II outputs zero to the integral regulator (block V), leading to $K_\lambda = K_{\lambda 0}$. If $\lambda_s^* < \lambda_{s\min}$, integral regulator begins to work and K_λ increases.
3) When rotor speed increases, the MI will increase too. Once MI is larger than the upper limitation of hysteresis comparator (block IV), the input of integral regulator is switched to zero, keeping λ_s^* unchanged. The two limitations of block IV are set to numbers near 1 such as 0.95 and 1.05, respectively. The expression of MI is (11)

$$\mathrm{MI} = \frac{V_s}{\frac{2}{\pi}V_{\mathrm{dc}}}. \tag{11}$$

When λ_s^* and MI meet with (12), Fig. 2 can be simplified into Fig. 4. In Fig. 4, $\lambda_{s\min}$ and λ_s^* are the input and output variables, respectively. k_i is the integral coefficient and $\lambda_{s\max}$ is a constant coefficient. $K_{\lambda 0}$ is regarded as a constant disturbance, which should be eliminated here.

$$\begin{cases} \lambda_s^* < \lambda_{s\min} \\ \mathrm{MI} < \mathrm{MI}_{\mathrm{lim}} \end{cases}. \tag{12}$$

We can derive (13) and (14) from Fig. 4. Substituting (13) to (14), the transfer function of Fig. 4 is obtained as (15). Equation (15) shows λ_s^* contains two parts: the first part is related to $K_{\lambda 0}$, and the second part is related to $\lambda_{s\min}$. Because $K_{\lambda 0}$ is designed as an initial value of K_λ and it is useful only as (12) is not met, it should be eliminated by the algorithm in Fig. 4. On the contrary, $\lambda_{s\min}$ is a very important input that should be followed by λ_s^*

$$K_\lambda(s) = K_{\lambda 0} + \frac{k_i}{s}\left(\lambda_s^*(s) - \lambda_{s\min}(s)\right) \tag{13}$$

$$\lambda_s^*(s) = \lambda_{s\max} K_\lambda(s) \tag{14}$$

$$\lambda_s^*(s) = \frac{\lambda_{s\max} s}{s - \lambda_{s\max} k_i} K_{\lambda 0} + \frac{-\lambda_{s\max} k_i}{s - \lambda_{s\max} k_i}\lambda_{s\min}(s). \tag{15}$$

In order to analyze the characteristic of the transfer function (15), a step command is given to $\lambda_{s\min}$ as shown in (16). The Laplace expression of this signal is like (17). Applying the final-value theorem to (15), the result is shown like (18). This equation illustrates that finally the first part will be pressed to zero and the second part will approach to λ_1. Therefore, the steady λ_s^* in whole range is shown in (19). In this equation, the stator flux linkage adjustment algorithm can be regarded as a segmented optimization method. λ_s^* has different values according to the $\lambda_{s\min}$ and MI

$$\lambda_{s\min} = \begin{cases} 0 & t = 0 \\ \lambda_1 & t > 0 \end{cases} \tag{16}$$

$$\lambda_{s\min}(s) = \frac{\lambda_1}{s} \tag{17}$$

$$\begin{aligned} \lambda_s^*(t)|_{t\to\infty} &= s\lambda_s^*(s)|_{s\to 0} \\ &= \frac{\lambda_{s\max} s^2}{s - \lambda_{s\max} k_i} K_{\lambda 0}\bigg|_{s\to 0} + \frac{-\lambda_{s\max} k_i}{s - \lambda_{s\max} k_i}\lambda_1\bigg|_{s\to 0} \\ &= \lambda_1 \end{aligned} \tag{18}$$

$$\lambda_s^* = \begin{cases} K_{\lambda 0}\lambda_{s\max} & (\lambda_s^* > \lambda_{s\min} \text{ and } \mathrm{MI} < \mathrm{MI}_{\mathrm{lim}}) \\ \lambda_{s\min} & (\lambda_s^* < \lambda_{s\min} \text{ and } \mathrm{MI} < \mathrm{MI}_{\mathrm{lim}}) \\ \text{hold} & (\mathrm{MI} > \mathrm{MI}_{\mathrm{lim}}) \end{cases}. \tag{19}$$

IV. Current LUTs and Voltage Overmodulation

A. Current Commands LUTs

The current commands (i_d^*, i_q^*) can be calculated from (6) and (9) according to the specific electromagnetic torque commands (T_e^*) and stator flux linkage commands (λ_s^*), using numerical calculation methods. But these methods are not only time-consuming but also sensitive to motor parameters. When the flux linkage is saturated, *d*-axis and *q*-axis inductances and permanent-magnet flux linkage will change significantly, which increases the difficulty of deriving i_d^* and i_q^* from (6) and (9). Exact measurements of L_d, L_q, and λ_f are difficult due to the limited accuracy of testing equipment and the cross-coupling effect of *d*-axis and *q*-axis inductances. Another way to obtain the nonlinear motor parameters is using finite element analysis, which is also time-consuming and the exact motor dimension is needed.

The LUT is constructed based on measured results in this paper. The load motor drives IPMSM at 600 r/min for two reasons: one is that the speed must be lower than the rated speed (700 r/min) to prevent saturation of output voltage, the other is that the speed must be as high as possible to decrease the influence of measurement error. *D*-axis and *q*-axis currents of IPMSM are controlled to follow a series of testing points shown as (20) [23], [35].

Stator flux linkage λ_s is calculated using (21), using measured rotor speed and voltage references. Equation (21) is based on (1) and (2) but deletes the addendum of stator resistance. It makes the λ_s more reasonable because the obtaining of λ_s^* from the algorithm in Fig. 2 is also under the condition of ignoring resistance. The λ_s in LUT must be consistent with the λ_s from the stator flux linkage adjustment algorithm. In fact, the λ_s is a composite variable, which includes the actual stator flux linkage as well as the "flux linkage" converted from

TABLE I
LUT STRUCTURE FOR PROPOSED METHOD

	λ_{s1}	λ_{s2}	$\cdots$	λ_{sn}
T_1	i_d^*, i_q^*	i_d^*, i_q^*	$\cdots$	i_d^*, i_q^*
T_2	$\cdots$	$\cdots$	$\cdots$	$\cdots$
.	$\cdots$	$\cdots$	$\cdots$	$\cdots$
.	$\cdots$	$\cdots$	$\cdots$	$\cdots$
T_n	$\cdots$	$\cdots$	$\cdots$	$\cdots$

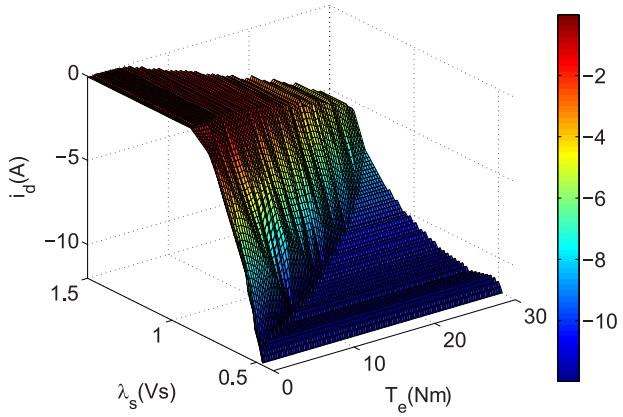

Fig. 5. i_d as a function of λ_s and T_e.

resistant voltage drop.

$$\begin{cases} i_d^* = -i_s \sin\theta \\ i_q^* = i_s \cos\theta \end{cases} \quad \begin{pmatrix} \theta = 10^\circ, 20^\circ, \ldots, 90^\circ \\ i_s = 1\text{A}, 2\text{A}, \ldots, 12\text{A} \end{pmatrix} \tag{20}$$

$$\lambda_s = \sqrt{\lambda_d^2 + \lambda_q^2} = \sqrt{\left(\frac{u_q}{\omega_e}\right)^2 + \left(\frac{-u_d}{\omega_e}\right)^2} = \frac{\sqrt{u_d^2 + u_q^2}}{\omega_e}. \tag{21}$$

The LUT can be constructed easily using i_d and i_q at each testing point with corresponding calculated λ_s and measured T_e. The structure of LUT used in the control algorithm is shown as Table I. Every row of LUT represents current commands with same torque and every column represents current commands with same stator flux linkage. Adjacent rows or columns have the same intervals. Although some combinations of i_d^* and i_q^* in Table I can be derived by linear interpolation of measured torque and stator flux linkage, some combinations cannot be obtained directly for the limitation of maximum torque and current as well as minimum stator flux linkage. When the elements are located outside the current limitation circle, current combination located on the current limitation circle with the same torque value is chosen as a replacement. Furthermore, current combinations on the right-hand side of the MTPA curve are not the optimal current commands, therefore, they are replaced by the current combinations located on the MTPA curve.

After the essential expansion and modification of the original LUT, the new LUT is finished and illustrated in Figs. 5 and 6. When the stator flux linkage command or torque command are out of range, a limitation will be added to the commands. Because the LUT data are finite, 2-D linear interpolation is utilized to calculate the i_d^* and i_q^* of a specific combination of λ_s^* and T_e^* [35].

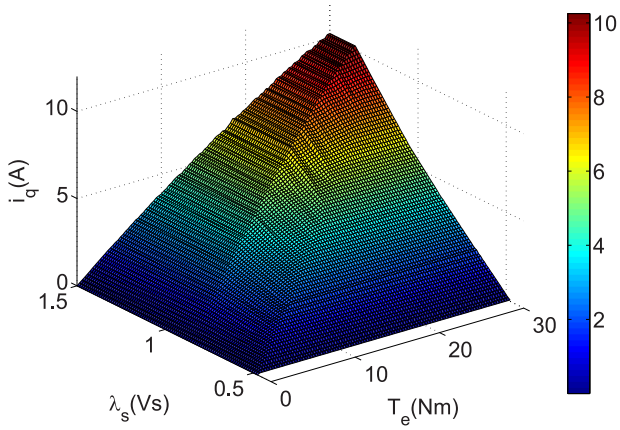

Fig. 6. i_q as a function of λ_s and T_e.

TABLE II
PARAMETERS OF IPMSM DRIVE SYSTEM

Variable name	Value
Rated power	3 kW
V_{dc}	300 V
Number of poles	4
Stator resistance per phase	4.3 Ω
λ_f	0.836 Vs
L_d	62 mH
L_q	119 mH
Rated speed	700 r/min
Rated current peak	12 A
Carrier frequent	5 kHz

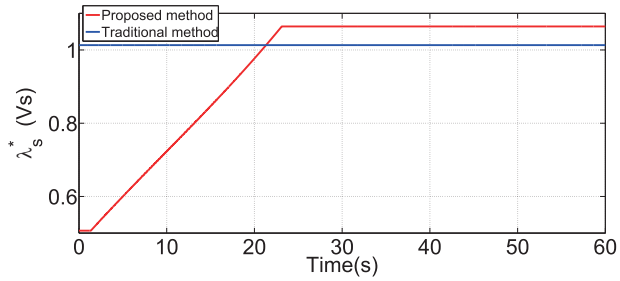

Fig. 7. Simulation results of λ_s^* for the proposed and traditional method.

B. Current Control and Overmodulation

Current regulator block uses the typical PI regulator with back EMF decouple and antiwindup [10], [36], [37]. The decouple part can improve the dynamic performance. The antiwindup part, on the contrary, prevents output voltage of current regulator from saturation. Because this part will weaken the function of integral regulator as MI near 1, the switch-ON point of hysteresis comparator in Fig. 2 is set a little larger than 1, which ensures that six-step operation mode can be achieved.

When voltage command vectors increase from the linear region to the outside of voltage hexagon, a smooth voltage transformation from PWM mode to six-step mode is achieved. The overmodulation method in [33] and [34] is used in this paper.

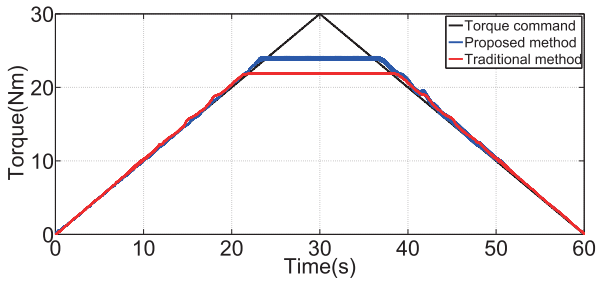

Fig. 8. Torque performances of proposed and traditional method.

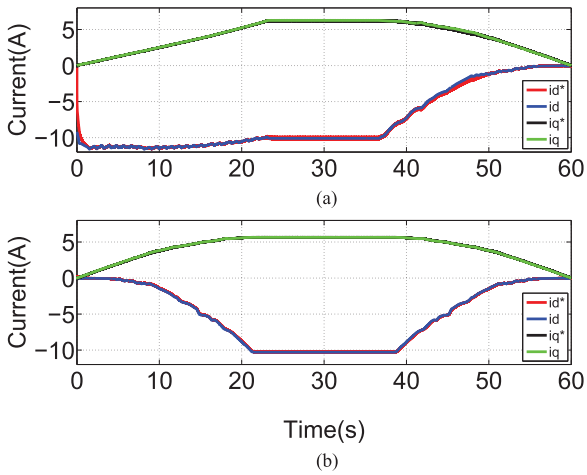

Fig. 9. d- and q-axis current commands and simulated currents. (a) Proposed method. (b) Traditional method.

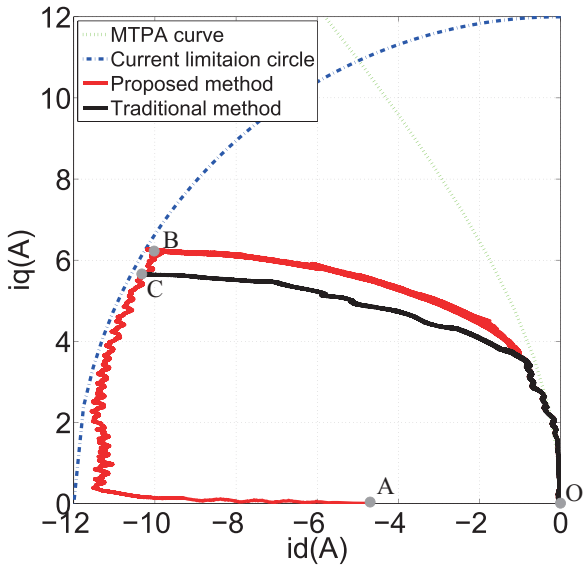

Fig. 10. Simulated i_d, i_q current trajectories of the proposed and traditional method.

The method proposed in [34] divides the overmodulation range into two parts. In part I (0.9069 < MI < 0.9517), only magnitude of voltage vector magnifies. However, in part II (0.9517 < MI < 1), both magnitude and angle of the original voltage vector are changed. When MI is larger than 1, the output voltage changes to six-step waveform.

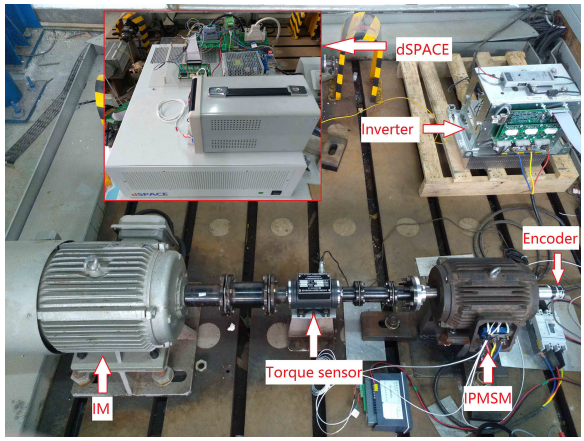

Fig. 11. Experimental setup.

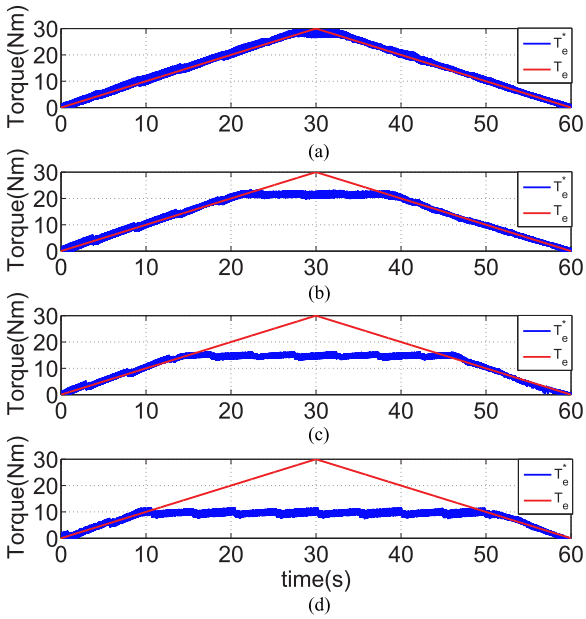

Fig. 12. Torque performances of proposed algorithm at different speeds. (a) n = 690 r/min. (b) n = 900 r/min. (c) n = 1110 r/min. (d) n = 1200 r/min.

V. Simulation Results

In the simulation, the IPMSM's parameters are shown in Table II and MATLAB/Simulink is used. The motor speed is set at a constant speed of 900 r/min. Ramp torque command increases from 0 to 30 N·m in 0–30 s and decreases from 30 to 0 N·m in 30–60 s. Simulations are carried out using two different methods. For the first simulation, the λ_s^* is derived from the proposed stator flux linkage commands adjustment algorithm shown in Fig. 2. K_λ is equal to $K_{\lambda 0}$ when the integral condition is not satisfied. The value of $K_{\lambda 0}$ is not important because K_λ will increase to a suitable value with the help of integrator. The second simulation adopts the traditional algorithm to calculate λ_s^* using (10).

Fig. 7 shows the change of λ_s^* for the two methods. In the traditional method, λ_s^* is equal to 1.01 Vs constantly because it is calculated from (10), in which both $V_{\rm dc}$ and ω_e are constant. In the proposed method, λ_s^* is about 0.5 Vs at first but starts to

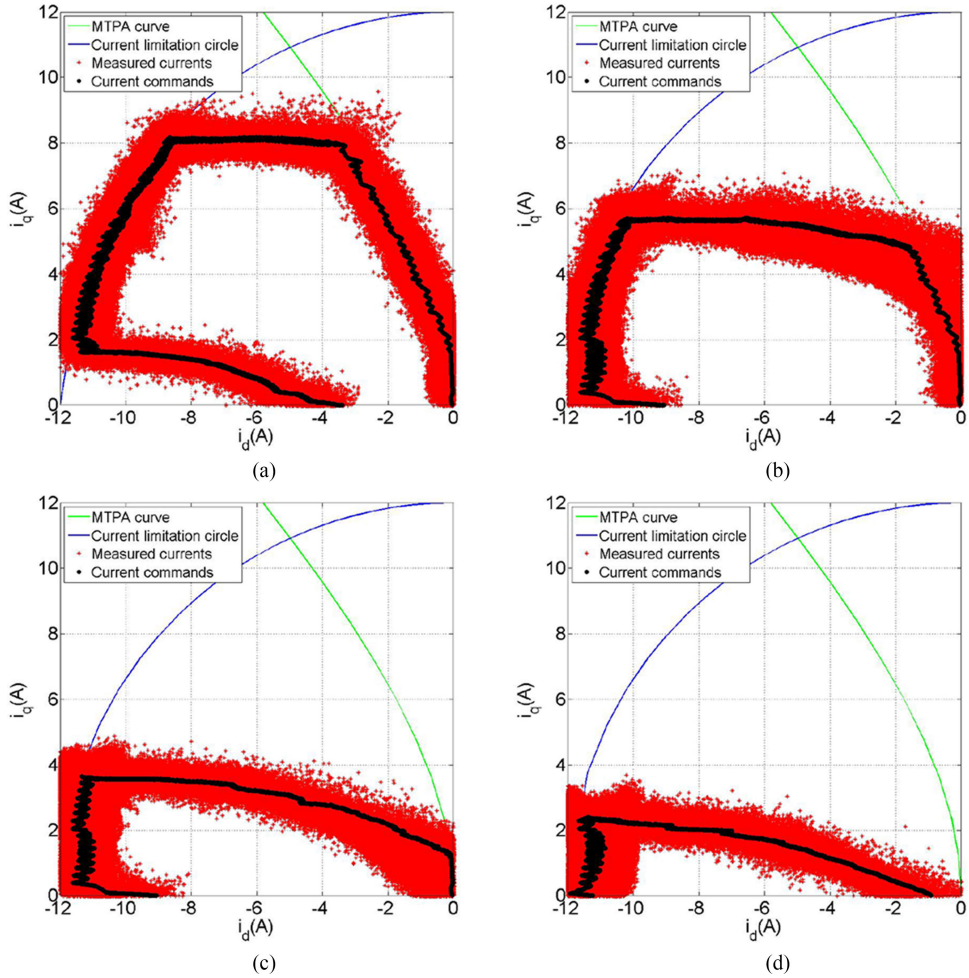

Fig. 13. Current tracks of proposed algorithm under (a) 690, (b) 900, (c) 1110, and (d) 1200 r/min.

increase as T_e^* reaches to 1.35 N·m. At this moment, $\lambda_{s\,\min}$ is larger than λ_s^*, which leads to the operation of integrator and the increase of K_λ. λ_s^* increases to 1.06 Vs and then holds unchanged as T_e^* is 23.1 N·m. At this moment, MI increases to $\mathrm{MI}_{\lim}$ and the integrator stops.

The difference of λ_s^* for the two methods leads to different torque performances as shown in Fig. 8. The proposed method can generate larger torque than the traditional one, which owes to the proposed stator flux linkage commands adjustment algorithm. The proposed method adjusts the λ_s^* to an optimal value which keeps a balance between preventing voltage saturation and maximizing torque output. The simulated torque cannot match well with the torque command during 15–25 N·m. This is caused by the mismatch between the measure-based LUTs and ideal motor model. Therefore, this torque error will not appear in the experimental results.

Fig. 9 compares the simulated currents of the proposed method and the traditional method. All of them can follow the commands, and the obvious difference between the two methods is the *d*-axis current before 30 s. The proposed method has much larger *d*-axis current magnitude before 30 s because the λ_s^* is smaller than that in traditional method.

Plotting the simulated currents in the *d*–*q* coordinate like Fig. 10 can reveal more difference between the proposed method and the traditional method. The current trajectory of proposed method is from A to B in 0–30 s and from B to O in 30–60 s. For the traditional method, the current trajectory moves from O to C in 0–30 s and moves back from C to O in 30–60 s. Points B and C represent the currents of maximum torque for the proposed and traditional method, respectively. Point B has larger i_q than point C, which means the proposed method has larger torque output ability than the traditional one.

VI. Experimental Results

The test rig is set up as shown in Fig. 11 to verify the effectiveness of proposed method, and the related parameters are listed in Table II. The IPMSM is coupled with an induction motor (IM), which is controlled in the speed mode. The inverter is controlled by dSPACE. The LUT illustrated in Figs. 5 and 6 is used in the control algorithm.

In order to illustrate the performance of proposed control algorithm, experiments are carried out under four different speeds: 690, 900, 1110, and 1200 r/min. The rotor of IPMSM is driven

by the IM with a constant speed. A rising ramp of torque command from 0–30 N·m and a declining ramp from 30–0 N·m are applied to the IPMSM. The torque performances at different speeds are shown in Fig. 12. T_e is measured by a torque sensor, but it is only used for result observation instead of a feedback signal in the control algorithm. When the speed is 690 r/min which is near the rated speed, the torque can follow the torque command during the whole period except a small error near 30 N·m. This is caused by the dc-link voltage drop. With the dc-link current increase, the dc-link voltage provided by the diode rectifier has an obvious drop from 310 to 270 V. Comparing Fig. 12(a)–(d), the maximum torque decreases gradually with the speed increase, but it is kept stable at its maximum value without obvious fluctuation.

The current tracks in the *d–q* coordinate for the four conditions above are shown in Fig. 13. First, all the four subfigures in Fig. 13 show that actual currents can follow the references well no matter what the speed is. Even when the speed is 1200 r/min and all the currents are located in the flux-weakening region, the measured current track still matches well with the references. Second, an obvious shrinking trend of voltage ellipse can be seen as the speed increases, which forces current tracks move from MTPA curve to flux-weakening region. When the voltage ellipse has intersection with the MTPA curve [see Fig. 13(a)–(c)], the current tracks are along the MTPA curve when the torque command is small, which ensures the minimum copper loss.

VII. Conclusion

In this paper, an improved torque feedforward flux weakening control method of IPMSMs is proposed. A current commands LUT based on measured data is constructed, which makes the control method independent from motor parameters. The stator flux linkage commands adjustment algorithm introduces an autoscaling coefficient, maximizing the output torque and improving torque stability in the flux-weakening field. Simulation and experimental results prove the effectiveness of the proposed algorithm.

References

[1] G. Pellegrino, A. Vagati, P. Guglielmi, and B. Boazzo, "Performance comparison between surface-mounted and interior PM motor drives for electric vehicle application," *IEEE Trans. Ind. Electron.*, vol. 59, no. 2, pp. 803–811, Feb. 2012.

[2] H. Nakai, H. Ohtani, E. Satoh, and Y. Inaguma, "Development and testing of the torque control for the permanent-magnet synchronous motor," *IEEE Trans. Ind. Electron.*, vol. 52, no. 3, pp. 800–806, Jun. 2005.

[3] B. Stumberger, G. Stumberger, D. Dolinar, A. Hamler, and M. Trlep, "Evaluation of saturation and cross-magnetization effects in interior permanent-magnet synchronous motor," *IEEE Trans. Ind. Appl.*, vol. 39, no. 5, pp. 1264–1271, Sep./Oct. 2003.

[4] T. M. Jahns, "Flux-weakening regime operation of an interior permanent-magnet synchronous motor drive," *IEEE Trans. Ind. Appl.*, vol. IA-23, no. 4, pp. 681–689, Jul. 1987.

[5] S. D. Sudhoff, K. A. Corzine, and H. J. Hegner, "A flux-weakening strategy for current-regulated surface-mounted permanent-magnet machine drives," *IEEE Trans. Energy Convers.*, vol. 10, no. 3, pp. 431–437, Sep. 1995.

[6] T. S. Kwon and S. K. Sul, "Novel antiwindup of a current regulator of a surface-mounted permanent-magnet motor for flux-weakening control," *IEEE Trans. Ind. Appl.*, vol. 42, no. 5, pp. 1293–1300, Sep./Oct. 2006.

[7] J.-M. Kim and S.-K. Sul, "Speed control of interior permanent magnet synchronous motor drive for the flux weakening operation," *IEEE Trans. Ind. Appl.*, vol. 33, no. 1, pp. 43–48, Jan./Feb. 1997.

[8] T.-s. Kwon and S.-K. Sul, "A novel flux weakening algorithm for surface mounted permanent magnet synchronous machines with infinite constant power speed ratio," in *Proc. Int. Conf. Electr. Mach. Syst.*, Oct. 2007, pp. 440–445.

[9] P. Y. Lin and Y. S. Lai, "Voltage control technique for the extension of dc-link voltage utilization of finite-speed SPMSM drives," *IEEE Trans. Ind. Electron.*, vol. 59, no. 9, pp. 3392–3402, Sep. 2012.

[10] Y. C. Kwon, S. Kim, and S. K. Sul, "Voltage feedback current control scheme for improved transient performance of permanent magnet synchronous machine drives," *IEEE Trans. Ind. Electron.*, vol. 59, no. 9, pp. 3373–3382, Sep. 2012.

[11] J.-J. Chen and K.-P. Chin, "Minimum copper loss flux-weakening control of surface mounted permanent magnet synchronous motors," *IEEE Trans. Power Electron.*, vol. 18, no. 4, pp. 929–936, Jul. 2003.

[12] Z. Q. Zhu, Y. S. Chen, and D. Howe, "Online optimal flux-weakening control of permanent-magnet brushless ac drives," *IEEE Trans. Ind. Appl.*, vol. 36, no. 6, pp. 1661–1668, Nov./Dec. 2000.

[13] X. Fang, T. Hu, F. Lin, and Z. Yang, "A novel flux-weakening control method based on single current regulator for permanent magnet synchronous motor," in *Proc. Int. Power Electron. Conf.*, May 2014, pp. 335–340.

[14] T. Hu, F. Lin, K. Lin, X. Fang, and Z. Yang, "Flux-weakening control of PMSM based on single current regulator and variable q-axis voltage," in *Proc. 15th Int. Conf. Electr. Mach. Syst.*, Oct. 2012, pp. 1–6.

[15] Y. Zhang, L. Xu, M. K. G. Ven, S. Chi, and M. Illindala, "Experimental verification of deep field weakening operation of a 50-kw IPM machine by using single current regulator," *IEEE Trans. Ind. Appl.*, vol. 47, no. 1, pp. 128–133, Jan./Feb. 2011.

[16] L. Xu, Y. Zhang, and M. K. Guven, "A new method to optimize q-axis voltage for deep flux weakening control of IPM machines based on single current regulator," in *Proc. Int. Conf. Electr. Mach. Syst.*, Oct. 2008, pp. 2750–2754.

[17] S. R. Macminn and T. M. Jahns, "Control techniques for improved high-speed performance of interior pm synchronous motor drives," *IEEE Trans. Ind. Appl.*, vol. 27, no. 5, pp. 997–1004, Sep./Oct. 1991.

[18] S. Morimoto, M. Sanada, and Y. Takeda, "Wide-speed operation of interior permanent magnet synchronous motors with high-performance current regulator," *IEEE Trans. Ind. Appl.*, vol. 30, no. 4, pp. 920–926, Jul./Aug. 1994.

[19] S. Morimoto, M. Sanada, and Y. Takeda, "Effects and compensation of magnetic saturation in flux-weakening controlled permanent magnet synchronous motor drives," *IEEE Trans. Ind. Appl.*, vol. 30, no. 6, pp. 1632–1637, Nov./Dec. 1994, doi: 10.1109/TIA.1994.350318.

[20] S.-Y. Jung, J. Hong, and K. Nam, "Current minimizing torque control of the IPMSM using Ferrari's method," *IEEE Trans. Power Electron.*, vol. 28, no. 12, pp. 5603–5617, Dec. 2013.

[21] K. D. Hoang and H. K. A. Aorith, "Online control of IPMSM drives for traction applications considering machine parameter and inverter nonlinearities," *IEEE Trans. Transport. Electrific.*, vol. 1, no. 4, pp. 312–325, Dec. 2015.

[22] H. W. de Kock, A. J. Rix, and M. J. Kamper, "Optimal torque control of synchronous machines based on finite-element analysis," *IEEE Trans. Ind. Electron.*, vol. 57, no. 1, pp. 413–419, Jan. 2010.

[23] D. Hu and L. Xu, "Characterizing the torque lookup table of an IPM machine for automotive application," in *Proc. IEEE Conf. Expo Transport. Electrific. Asia-Pacific*, Aug. 2014, pp. 1–6.

[24] R. U. Lenke, R. W. De Doncker, M. S. Kwak, and T. S. Kwon, "Field weakening control of interior permanent magnet machine using improved current interpolation technique," in *Proc. 37th IEEE Power Electron. Spec. Conf.*, 2006, pp. 1–5.

[25] S. Morimoto, Y. Takeda, T. Hirasa, and K. Taniguchi, "Expansion of operating limits for permanent magnet motor by current vector control considering inverter capacity," *IEEE Trans. Ind. Appl.*, vol. 26, no. 5, pp. 866–871, Sep./Oct. 1990.

[26] J.-H. Lee *et al.*, "IPMSM torque control method considering dc-link voltage variation and friction torque for ev/hev applications," in *Proc. IEEE Veh. Power Propulsion Conf.*, Oct 2012, pp. 1063–1069.

[27] H. Ge, Y. Miao, B. Bilgin, B. Nahid-Mobarakeh, and A. Emadi, "Speed range extended maximum torque per ampere control for pm drives considering inverter and motor nonlinearities," *IEEE Trans. Power Electron.*, vol. 32, no. 9, pp. 7151–7159, Sep. 2017.

[28] T. S. Kwon, G. Y. Choi, M. S. Kwak, and S. K. Sul, "Novel flux-weakening control of an IPMSM for quasi-six-step operation," *IEEE Trans. Ind. Appl.*, vol. 44, no. 6, pp. 1722–1731, Nov./Dec. 2008.
[29] B. Cheng and T. R. Tesch, "Torque feedforward control technique for permanent-magnet synchronous motors," *IEEE Trans. Ind. Electron.*, vol. 57, no. 3, pp. 969–974, Mar. 2010.
[30] B.-H. Bae, N. Patel, S. Schulz, and S.-K. Sul, "New field weakening technique for high saliency interior permanent magnet motor," in *Proc. 38th IAS Annu. Meet. Conf. Rec. Ind. Appl. Conf.*, Oct. 2003, vol. 2, pp. 898–905.
[31] G. Y. Choi, M. S. Kwak, T. S. Kwon, and S. K. Sul, "Novel flux-weakening control of an IPMSM for quasi six-step operation," in *Proc. 42nd IAS Annu. Meet. Conf. Rec. Ind. Appl. Conf.*, Sep. 2007, pp. 1315–1321.
[32] L. Zhu and X. Wen, "A new precise torque control method of PMSMs in flux-weakening operation," in *Proc. IEEE Conf. Expo Transport. Electrific. Asia-Pacific*, Aug. 2014, pp. 1–4.
[33] J. Holtz, W. Lotzkat, and A. M. Khambadkone, "On continuous control of PWM inverters in the overmodulation range including the six-step mode," *IEEE Trans. Power Electron.*, vol. 8, no. 4, pp. 546–553, Oct. 1993.
[34] D. C. Lee and G. M. Lee, "A novel overmodulation technique for space-vector PWM inverters," *IEEE Trans. Power Electron.*, vol. 2, no. 6, pp. 1144–1151, Nov. 1998.
[35] D. Hu, Y. M. Alsmadi, and L. Xu, "High-fidelity nonlinear IPM modeling based on measured stator winding flux linkage," *IEEE Trans. Ind. Appl.*, vol. 51, no. 4, pp. 3012–3019, Jul./Aug. 2015.
[36] C. Bohn and D. P. Atherton, "An analysis package comparing PID anti-windup strategies," *IEEE Control Syst.*, vol. 15, no. 2, pp. 34–40, Apr. 1995.
[37] F. Briz, A. Diez, M. W. Degner, and R. D. Lorenz, "Current and flux regulation in field-weakening operation of induction motors," *IEEE Trans. Ind. Appl.*, vol. 37, no. 1, pp. 42–50, Jan./Feb. 2001.

Yuzheng Chen was born in Beijing, China, in 1992. He received the B.S. degree in electrical engineering from Zhejiang University, Hangzhou, China, in 2015. He is currently working toward the M.S. degree in electrical engineering with Zhejiang University.

His main research interest includes flux-weakening control of PMSM, especially for electric vehicles.

Xiaoyan Huang (M'09) received the B.E. degree in control measurement techniques and instrumentation from Zhejiang University, Hangzhou, China, in 2003, and the Ph.D. degree in electrical machines and drives from the University of Nottingham, Nottingham, U.K., in 2008.

From 2008 to 2009, she was a Research Fellow with the University of Nottingham. She is currently a Professor with the College of Electrical Engineering, Zhejiang University, Hangzhou, China, where she is working on electrical machines and drives. Her research interests include PM machines and drives for aerospace and traction applications, and generator system for urban networks.

Jun Wang (S'17) received the B.E. degree in electrical engineering from Zhejiang University, Hangzhou, China, in 2014. He is currently working toward the Ph.D. degree in electrical machines and drives with Zhejiang University, Hangzhou, China.

His research interests include control and drive system design for PMSM in the applications of electric vehicles.

Feng Niu (M'15) was born in Hebei, China, in 1986. He received the B.S. and Ph.D. degrees from the Hebei University of Technology, Tianjin, China, in 2009 and 2015, respectively, both in electrical engineering.

He is currently a Postdoctoral Fellow with the College of Electrical Engineering, Zhejiang University, Hangzhou, China. From September 2012 to September 2014, he was a Research Fellow with the Electrical Machines and Drives Laboratory, Michigan State University, East Lansing, MI, USA. His research interests include motor system and control, power converter control, and intelligent electrical equipment.

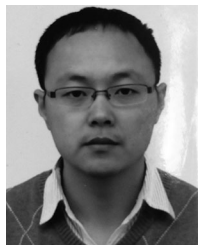

Jian Zhang received the Ph.D. degree in mechanical engineering in 2010 from Zhejiang University, Hangzhou, China.

He is currently an Assistant Professor of electrical engineering with Zhejiang University. His current research interests includes motor design and reliability analysis.

Youtong Fang (M'11–SM'15) received the B.S. and Ph.D. degrees in electrical engineering from Hebei University of Technology, Hebei, China, in 1984 and 2001, respectively.

He is currently a Professor with the College of Electrical Engineering, Zhejiang University, Hangzhou, China. His research interests include the application, control, and design of electrical machines.

Lijian Wu (M'11–SM'14) received the B.Eng. and M.Sc. degrees from the Hefei University of Technology, Hefei, China, in 2001 and 2004, respectively, and the Ph.D. degree from the University of Sheffield, Sheffield, U.K., in 2011, all in electrical engineering.

From 2004 to 2007, he was an Engineer with Delta Electronics (Shanghai) Co, Ltd. From 2012 to 2013, he was with Sheffield Siemens Wind Power Research Center as a Design Engineer focusing on wind power generators. From 2013 to 2016, he was an Advanced Engineer with Siemens Wind Power A/S in Denmark. Since 2016, he has been with Zhejiang University, Hangzhou, China, where he is currently a Professor of electrical machines and control systems. His current major research interests include design and control of permanent magnet machines.